

## Cross-sectional insight in the water evolution and transport in polymer electrolyte fuel cells

Christoph Hartnig,<sup>a)</sup> Ingo Manke, Robert Kuhn, Nikolay Kardjilov, John Banhart, and Werner Lehnert

Centre for Solar Energy and Hydrogen Research Baden-Württemberg, Helmholtzstraße 8, 89081 Ulm, Hahn-Meitner Institute Berlin, Glienicker Str. 100, 14109 Berlin, Germany

(Received 20 February 2008; accepted 19 March 2008; published online 4 April 2008)

The evolution of liquid water and its transport through the porous gas diffusion media in an operating fuel cell were investigated applying an experimental setup for high spatial resolution of  $3\ \mu\text{m}$ . Fundamental aspects of cluster formation in hydrophobic/hydrophilic porous materials as well as processes of multiphase flow are addressed. The obtained water distributions provide a detailed insight in the membrane electrode assembly and the porous electrode with regard on the existence and transport of liquid water. In addition, the results approve transport theories used within the framework of percolation theory and demonstrate the need for adapted modeling approaches.

© 2008 American Institute of Physics. [DOI: 10.1063/1.2907485]

In polymer electrolyte fuel cells, the chemical energy stored in hydrogen and oxygen is converted to electrical and thermal power.<sup>1,2</sup> A variety of factors influence the broad market introduction of fuel cells. The most striking ones besides the price of the fuel cells and low quantities are the long term stability and an optimum performance over a broad range of operating conditions.

The reactant gases, oxygen (usually supplied as air) and hydrogen, are distributed across the active area by means of a flow field on the anode and the cathode. In order to obtain a well distributed supply, an additional porous carbon fiber material [gas diffusion layer (GDL)] is applied which ensures the transport to the electrochemically active area. At the same time, product water stemming from the electrochemical reaction as well as the external humidification has to be removed the same diffusive way in which the reactant gases are transported to the catalyst layer.

Water is thereby predominantly formed at the cathode and plays a crucial role in the fuel cell operation. For the polymer electrolyte membrane, a certain humidity is necessary to keep the protonic conductivity of the polymer.<sup>3-7</sup> Water molecules are transported from the anode through the membrane to the cathode by the electro-osmotic drag which is balanced by back diffusion due to the gradient of the water concentration ensuring a sufficient humidification of the anode. Depending on the current density, one of the processes is favored above the other which will be addressed in more detail below. In the adjacent gas diffusion layer, water is transported in gas phase from the catalyst layer to the gas channels of the flow field at low current densities (or, in other words, at low water production rates). However, at high current densities the saturation pressure of water can be exceeded leading to the existence of two phases, water vapor and liquid water. The latter phase might lead to blocked pathways in the GDL and the catalyst layers which in turn limit the maximum achievable power density. These two-phase or even multiphase flow phenomena are not limited to fuel cell processes but play an important role in several natural and

technical processes as, e.g., water transport through pores in rocks and oil sands.<sup>8</sup>

Several approaches employing modified cells with transparent parts were proposed to visualize the through plane water transport.<sup>9-11</sup> However, such modifications lead to unpredictable interference with the water distribution. In view of the limitation of the spatial and time resolution to around  $50\ \mu\text{m}$  and a few minutes, respectively, neutron radiography is of limited use to gain a detailed cross-sectional view of the active area.<sup>12-14</sup>

Here, we present a detailed study of the water transport through the membrane electrode assembly (MEA) and GDL structure of a fuel cell. Emphasis was taken on the fuel cell setup which allows for a high spatial resolution of  $3\ \mu\text{m}$  applying synchrotron x-ray radiography and investigation of water transport phenomena that were not accessible up to now.<sup>15</sup>

A single channel fuel cell setup has been designed to fulfill two preconditions, the resemblance of a realistic system as well as the possibility to distinguish between the different components of the fuel cell and to gain a cross-sectional insight in the evolution and transport of water at high spatial resolution. The flow field with an electrochemically active area of  $12\ \text{cm}^2$  was machined in graphite composite material. SGL Sigracet 10 BB gas diffusion material with a poly-tetrafluorethylene (PTFE) loading of 5% was applied to both electrodes, and a GORE 5621 MEA with a membrane thickness of  $40\ \mu\text{m}$  was used with catalyst loadings of  $0.3\ \text{mg}/\text{cm}^2$  at the anode and  $0.4\ \text{mg}/\text{cm}^2$  at the cathode.<sup>16</sup> The upright positioned fuel cell was operated at standard parameter settings. The cathodic utilization rate  $u_C$  describing the fraction of gas consumed along the reactive area is set to  $u_C=25\%$ , the anodic utilization rate to  $u_A=90\%$ , and the temperature of the stack to  $T=60\ ^\circ\text{C}$ . The cathodic gas stream was humidified at a dew point of  $25\ ^\circ\text{C}$ , while the anode remained unhumidified. Ambient pressure was kept at the media outlets.

The experiments were performed at the tomography facility of the BAMline at the synchrotron BESSY (Berlin, Germany). A  $2048 \times 2048$  pixel camera (Princeton VersArray 2048B) was used to capture images up to  $7 \times 7\ \text{mm}^2$  large with corresponding image pixel sizes between 1.5 and

<sup>a)</sup> Author to whom correspondence should be addressed. Electronic mail: christoph.hartnig@zsw-bw.de.

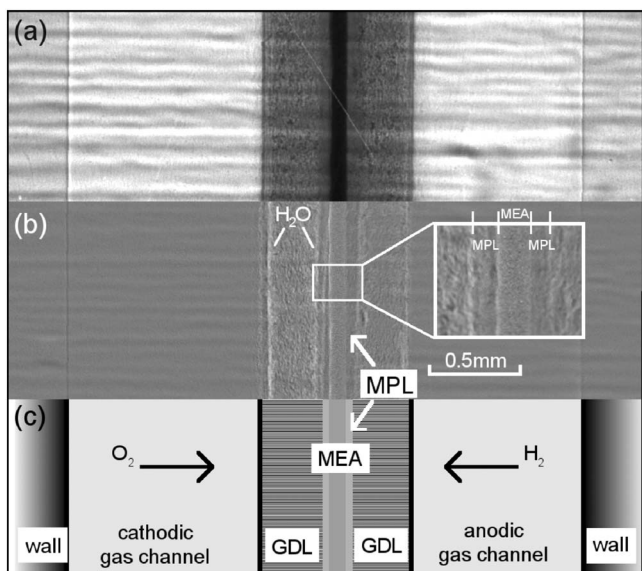


FIG. 1. Cross section of the fuel cell. (a) Unmodified image as obtained from synchrotron imaging. (b) Normalized image with respect to an empty (water-free) cell. Water agglomerates can be identified in this representation as bright spots. (c) Schematic drawing of the cell. To either side of the GDL/MEA, the gas channels and the back side of the flow fields are visible. Attached to the GDL towards the membrane is the hydrophobic MPL which can be recognized as fine grained structure in the inset.

$3.5 \mu\text{m}$  which correspond to a physical spatial resolution of  $3\text{--}7 \mu\text{m}$ . The measurement time per image was around 5 s, 1 s for exposure and 4 s for data readout.

In Fig. 1, a cross-sectional view of a fuel cell is displayed in which the individual components of a cell can be clearly differentiated. Images taken during the measurements are normalized with respect to a water-free (dry) cell. The unhumidified reactant gas flow is switched on and no electric load is applied so that no net water is produced. Figure 1(a) displays the image as obtained from the experiments. Figure 1(b) is derived from the normalization where components such as gaskets are subtracted and do not influence the results; water can hereby be identified as bright spots. In Fig. 1(c), a schematic drawing of the cell setup and the different components are displayed clarifying the different parts of the image. The core of the fuel cell, the MEA consisting of the perfluorinated sulfonic acid membrane with the catalyst attached on both sides in the centre of the cell, exhibits a high absorption coefficient. The central part of the image is magnified in the inset of Fig. 1(b). At both sides of the MEA are the GDLs. Attached on the GDL next to the MEA is a so-called microporous layer (MPL) which can be distinguished from the carbon fiber as a fine grained structure. The MPL mainly consists of carbon black and PTFE which results in a predominantly hydrophobic material ensuring an equilibrated water content of the catalytic area. Due to its microporous structure with very hydrophobic and therefore water-free spots caused by the PTFE, the MPL allows for the diffusion of reactant gases to the catalyst layer. To both sides of the GDLs, the cathodic and anodic flow field channels and the back wall of the flow field can be identified.

Normalized images of the fuel cell operating at different current densities are displayed in Fig. 2. The current density  $i_0$  determines the rate of water production; increasing  $i_0$  leads to enhanced water formation and vice versa. At low current densities [ $i_0=250 \text{ mA/cm}^2$ , Fig. 2(a)] hardly any liquid water can be detected. Product water from the electrochemical

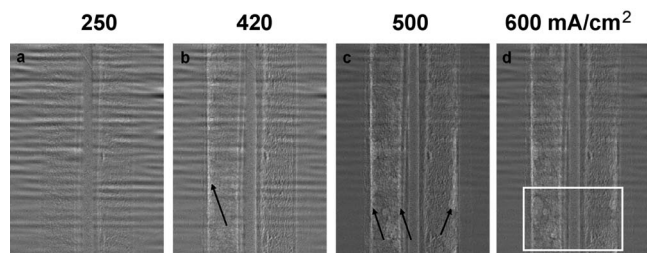


FIG. 2. Liquid water formation as function of current density  $i_0$ . (a) At  $i_0=250 \text{ mA/cm}^2$ , hardly any liquid water is formed. (b) Larger values of  $i_0$  ( $420 \text{ mA/cm}^2$ ) lead to initial water clusters on the cathode (white spots, arrow). (c) Water clusters appear at the anode at  $i_0=500 \text{ mA/cm}^2$  (arrows denote preferred condensation spots). (d) Water clusters are present to a large extent in both gas diffusion electrodes at  $i_0=500 \text{ mA/cm}^2$ . Horizontal stripes are artifacts caused by thermal fluctuation of the monochromator setup. The white box depicts the area used to quantify the water content as displayed in Fig. 3.

reaction is mainly transported in gas phase, phenomena such as two-phase flow do not play a significant role at these operating conditions. With increasing current density [ $i_0=420 \text{ mA/cm}^2$ , Fig. 2(b)] liquid water primarily appears in the cathodic GDL which is the place where the protons transported through the membrane recombine with the reaction products of the oxygen reduction reaction to form liquid water. At higher current densities, both at the anodic and cathodic side liquid water is observed [ $i_0>500 \text{ mA/cm}^2$ , Figs. 2(c) and 2(d)] resulting from the back diffusion due to the water gradient between anode and cathode. Two main positions of liquid water agglomerations can be estimated along the cross section. The first one is located close to the gas channel and the second one next to the MPL. Due to its hydrophobic nature, the MPL contains hardly any liquid water. In both cases, the liquid water is located in the area beneath the ribs of the flow field, forming a diffusion barrier for the reactant gases. The further transport of these agglomerates can either take place in gas phase or in liquid phase and is subject of ongoing research activities.

Liquid water agglomerates were quantified by summation of 100 rows along the marked area in Fig. 2. The relative amounts along the cross section as a function of  $i_0$  are displayed in Fig. 3. As already estimated qualitatively from Fig. 2, at low current densities, only small amounts of water condense in the vicinity of the MPL indicating an almost liquid water-free situation. At higher current densities, larger

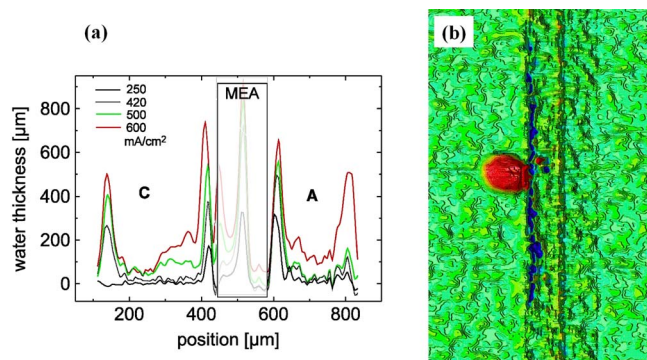


FIG. 3. (Color online) (a) Quantification and location of liquid water in the cathodic (C) and anodic (A) gas diffusion layer. Depending on the operating conditions, one or two diffusion barriers formed by liquid water can be detected. The water content of the MEA is shaded due to the low statistics caused by high absorption coefficients of platinum. (b) Eruptive water transport from the GDL to the gas channel.

clusters are formed. A first maximum of the liquid water distribution is located directly in the GDL in close proximity to the MPL. A second maximum resides beneath the rib next to the channel. The formation of these diffusion barriers can be explained by slight temperature differences between the electrochemically active area and the adjacent GDL and the MPL. Liquid water, which might exist at the catalyst surface, evaporates and diffuses through the MPL where, due to the high hydrophobicity, no condensation can take place. Once the water vapor reaches the GDL, the gas pressure of the water is exceeded and condensation on hydrophilic spots steps in next to the MPL. Mass transport limitations due to the external humidification support the condensation.

On the anode, a similar behavior can be observed. Contrary to the processes on the cathode, already at low current densities ( $i_0=300\text{--}400\text{ mA/cm}^2$ ) primary spots of liquid water accumulate in the porous media close to the MPL. With increasing values of  $i_0$  the amount of liquid water increases and a more or less dense layer is formed. A second diffusion barrier caused by liquid water as observed at the cathode is not observed at the anode where no transport limitations due to the humidification exist. Only at higher current densities ( $i_0>500\text{ mA/cm}^2$ ) a significant second peak is observed which is comparable to the one formed on the cathode. The maxima of the liquid water content close to the reaction layer appear higher at the anode for all but the highest investigated current density. The aforementioned balance between the back diffusion and the electro-osmotic drag is hinted at by this distribution: only at high current densities the back diffusion is outweighed by the electro-osmotic drag.

Besides the mere location of the agglomerates, the dynamics of the liquid water transport from the catalytic layer to the flow field channel is of major interest not only to shed light on the transport processes but to compare the mechanisms found to theoretical descriptions and estimate the contribution of multiphase flow phenomena to the overall transport. The transport of liquid water is elucidated in more detail in Fig. 3(b). Displayed is the difference between two consecutive images with a time resolution of 5 s at a current density at which liquid water is observed ( $i_0=500\text{ mA/cm}^2$ ). Within the observation period between two images, a water droplet was formed in the channel. Small water clusters incorporated in the prevalently hydrophobic GDL merge to form larger ones which finally erupt (“burst”) from the GDL to the gas transport channels.

A possible interpretation of the observed phenomena is based on a description as employed in geological disciplines. Compact cluster growth of a nonwetting liquid (water) in hydrophobic pores results from Haines jumps which are caused by interfacial advances in a quite localized section. The capillary pressure in the neighboring entity is lower than in the vicinity which causes the smaller clusters to burst to neighboring pores. The transition (avalanche) to the gas channel is triggered by the same factors, whereas for this process an additional mechanism can be observed. The bursting droplet carries away water from the GDL and the “supply” is not sufficient to fill the pores. These choke offs lead to empty pores which are filled afterwards and the cycle starts again.<sup>17,18</sup>

We have investigated the cross-sectional transport of liquid water in porous gas diffusion materials as employed in low temperature fuel cells by means of synchrotron x-ray radiography with a spatial resolution of 3  $\mu\text{m}$  and a time resolution of 5 s. The investigations provide insights into multiphase water transport phenomena that were not accessible up to now. The water distribution in the GDL strongly depends on the water production rate (the current density) and up to two different diffusion barriers caused by liquid water were detected at high current densities. The position of these diffusion barriers depends on the hydrophobic/hydrophilic properties of the employed materials. The microscopic transport of liquid water might be described by a series of collapses of smaller droplets leading to a compact water cluster growth in the GDL. At the transition from the GDL to the gas channel, choke-off effects cause emptied pores which are filled gradually and lead to a cyclic transport behavior.

The presented finding might serve as basis to develop tailor-made materials with customized properties to remove excess liquid water more efficiently. Modeling approaches of multiphase flows can be adapted based on these results and estimations on the amount of liquid water involved in the overall water transport might be deduced.

C.H. would like to thank Frank Häußler and Joachim Scholta for their support at constructing the fuel cell and Sebastian Kleinau for supporting the measurements and fruitful discussions. The research activities were funded by the German Federal Ministry for Education and Science (BMBF) under Grant Nos. 03SF0324A and 03SF0324F.

<sup>1</sup>B. Steele and A. Heinzl, *Nature (London)* **414**, 345 (2001).

<sup>2</sup>F. Bruijn, *Green Chem.* **7**, 132–150 (2005).

<sup>3</sup>M. Eikerling, S. J. Paddison, L. R. Pratt, and T. A. Zawodzinski, *Chem. Phys. Lett.* **368**, 108 (2003).

<sup>4</sup>H. L. Yeager and A. Steck, *J. Electrochem. Soc.* **128**, 1880 (1991).

<sup>5</sup>K. D. Kreuer, S. J. Paddison, E. Spohr, and M. Schuster, *Chem. Rev. (Washington, D.C.)* **104**, 4637 (2004).

<sup>6</sup>G. Gebel, *Polymer* **41**, 5829 (2000).

<sup>7</sup>P. W. Majsztrik, M. B. Satterfield, A. B. Bocarsly, and J. B. Benziger, *J. Membr. Sci.* **301**, 93 (2007).

<sup>8</sup>C.-Y. Wang and P. Cheng, *Int. J. Heat Mass Transfer* **39**, 3607 (1996).

<sup>9</sup>K. Tüber, D. Pócza, and C. Hebling, *J. Power Sources* **124**, 403 (2003).

<sup>10</sup>P. Argyropoulos, K. Scott, and W. M. Taama, *Electrochim. Acta* **44**, 3575 (1999).

<sup>11</sup>D. Spornjak, A. K. Prasad, and S. G. Advani, *J. Power Sources* **170**, 334 (2007).

<sup>12</sup>R. Satija, D. L. Jacobson, M. Arif, and S. A. Werner, *J. Power Sources* **129**, 238 (2004).

<sup>13</sup>A. Turhan, K. Heller, J. S. Brenizer, and M. M. Mench, *J. Power Sources* **160**, 1195 (2006).

<sup>14</sup>A. B. Geiger, A. B. Geiger, A. Tsukada, E. Lehmann, P. Vontobel, A. Wokaun, and G. G. Scherer, *Fuel Cells* **2**, 92 (2002).

<sup>15</sup>I. Manke, Ch. Hartnig, M. Grünerbel, W. Lehnert, N. Kardjilov, A. Haibel, A. Hilger, J. Banhart, and H. Riesemeier, *Appl. Phys. Lett.* **90**, 174105 (2007).

<sup>16</sup>Certain trade names and products are mentioned in the text in order to specify the experimental setup and procedure. In no case does such an identification imply recommendation or endorsement nor does it imply that these materials are necessarily the best available for the application.

<sup>17</sup>L. Paterson, A. P. Sheppard, and M. A. Knackstedt, *Phys. Rev. E* **66**, 035101 (2002).

<sup>18</sup>M. Ferer, G. S. Bromhal, and D. H. Smith, *Physica A* **311**, 5 (2002).